Received: 12 June 2020 | Accepted: 21 September 2020

DOI: 10.1002/pld3.275

ORIGINAL RESEARCH

High affinity Na^+ transport by wheat HKT1;5 is blocked by K^+

Bo Xu[1,2] | Maria Hrmova[2,3] | Matthew Gilliham[1,2]

[1]Australian Research Council Centre of Excellence in Plant Energy Biology, University of Adelaide, Waite Research Precinct, Glen Osmond, SA, Australia

[2]School of Agriculture, Food and Wine, and Waite Research Institute, University of Adelaide, Waite Research Precinct, Glen Osmond, SA, Australia

[3]School of Life Science, Huaiyin Normal University, Huai'an, China

Correspondence
Matthew Gilliham, Australian Research Council Centre of Excellence in Plant Energy Biology, University of Adelaide, Waite Research Precinct, Glen Osmond, SA, Australia.
Email: matthew.gilliham@adelaide.edu.au

Funding information
This work was supported by funding to M.G. from the Grains Research and Development Corporation (UA00145), the Australian Research Council through the Centre of Excellence (CE1400008) and Future Fellowship (FT130100709) schemes, and by funding to M.H. from the Australian Research Council (DP120100900) and the Huaiyin Normal University (China).

Abstract

The wheat sodium transporters TmHKT1;5-A and TaHKT1;5-D are encoded by genes underlying the major shoot Na^+ exclusion loci *Nax2* and *Kna1* from *Triticum monococcum* (Tm) and *Triticum aestivum* (Ta), respectively. In contrast to HKT2 transporters that have been shown to exhibit high affinity K^+-dependent Na^+ transport, HKT1 proteins have, with one exception, only been shown to catalyze low affinity Na^+ transport and no K^+ transport. Here, using heterologous expression in *Xenopus laevis* oocytes we uncover a novel property of HKT1 proteins, that both TmHKT1;5-A and TaHKT1;5-D encode dual (high and low) affinity Na^+-transporters with the high-affinity component being abolished when external K^+ is in excess of external Na^+. Three-dimensional structural modeling suggested that, compared to Na^+, K^+ is bound more tightly in the selectivity filter region by means of additional van der Waals forces, which is likely to explain the K^+ block at the molecular level. The low-affinity component for Na^+ transport of TmHKT1;5-A had a lower K_m than that of TaHKT1;5-D and was less sensitive to external K^+. We propose that these properties contribute towards the improvements in shoot Na^+-exclusion and crop plant salt tolerance following the introgression of TmHKT1;5-A into diverse wheat backgrounds.

KEYWORDS

salinity, high-affinity K transporters, membrane transport, KtrB, dual affinity, sodium exclusion

1 | INTRODUCTION

Crops suffer reduced growth and grain yield under salinity stress. Salt, when it builds up to high concentrations in the growing medium (i.e., soil solution) imposes an osmotic limitation on water uptake, interferes with optimal nutrient homeostasis, induces numerous signaling events and leads to the accumulation of high leaf sodium (Na^+) concentrations, which is proposed to cause either an ionic toxicity or an energy crisis due to insufficient energy being generated through photosynthesis and carbon assimilation in plants (Munns and Gilliham, 2015; Munns et al., 2020; van Zelm et al., 2020).

Exclusion of Na^+ from leaves is often cited as a major mechanism contributing toward the salinity tolerance of many economically important crops including the cereals rice (*Oryza sativa*) and wheat (*Triticum aestivum* and *Triticum monococcum*) (Munns and Gilliham, 2015; Munns et al., 2020; van Zelm et al., 2020), with the High-affinity potassium (K^+) transporter (HKT) protein family having a major role in this trait (Ren et al., 2005; James et al., 2006; Munns et al., 2012; Campbell et al., 2017; Ismail and Horie, 2017; Henderson et al., 2018; Xu et al., 2018; Cao et al., 2019; Wu et al., 2020). This family of proteins is present in all plants so far sequenced; more broadly the members of the high affinity K^+/Na^+ transporting Ktr/

TrK/HKT superfamily of proteins are present in bacteria (Ktr and TrK), fungi (TrK) and plants (HKT) (Sentenac and Bonneaud, 1992; Corratgé-Faillie et al., 2010).

These plant HKTs are divided into two clades: (a) class 1 HKT proteins (HKT1;x) are mostly Na^{+}-selective transporters; (b) whereas class 2 HKTs (HKT2;y) mostly function as K^{+}-Na^{+} symporters and so far have been only identified in cereal monocots (Asins et al., 2013; Waters et al., 2013). This definition has been challenged on occasion, such as for OsHKT2;4, where following its characterization in *Xenopus laevis* oocytes, there are conflicting reports on its permeability to Ca^{2+}, Mg^{2+}, and NH_4^{+} in addition to K^{+} and Na^{+} (Lan et al., 2010; Horie et al., 2011; Sassi et al., 2012). Furthermore, there are two reports of K^{+} permeability in the HKT1 clade. Firstly, *Arabidopsis* AtHKT1 could complement K^{+} transport deficient *E. coli*, although no K^{+} permeability could be found when *AtHKT1* was expressed in *X. laevis* oocytes in the same study (Uozumi et al., 2000). Secondly, *Eucalyptus camaldulensis* EcHKT1;1 and EcHKT1;2, which appear to be the exception for the HKT1 proteins characterized so far in that they transport both Na^{+} and K^{+} when expressed in *X. laevis* oocytes (Liu et al., 2001). Other HKT1 transporters have no reported K^{+} permeability (Uozumi et al., 2000; Mäser et al., 2002; Platten et al., 2006; Jabnoune et al., 2009; Cotsaftis et al., 2012; Munns et al., 2012; Waters et al., 2013; Byrt et al., 2014; Campbell et al., 2017).

Whilst K^{+} transport is not a common feature of HKT1 transporters, several have shown the property of K^{+}-regulated Na^{+} transport (Ben Amar et al., 2013; Almeida et al., 2014a; Almeida et al., 2014b; Byrt et al., 2014). For instance, the presence of 10 mM external K^{+} ($[K^{+}]_{ext}$) reduced the inward Na^{+} current of *X. laevis* oocytes expressing *HKT1;5* from *T. aestivum* (*TaHKT1;5-D*) (Byrt et al., 2014), and reduced outward Na^{+} currents generated by expression of *HKT1;2* from *Solanum lycopersicum* (*SlHKT1;2*) (Almeida et al., 2014a). Interestingly, $[K^{+}]_{ext}$ stimulated both inward and outward Na^{+} transport of *X. laevis* oocytes expressing two *HKT1;4* alleles from *Triticum turgidum* L. subsp. *Durum*, when assayed with solutions of very low ionic strength (Ben Amar et al., 2013).

Ktr/TrK/HKT proteins are predicted to consist of eight transmembrane α-helices that adopt pseudo-four-fold symmetry along a central pore (Mäser et al., 2002; Cotsaftis et al., 2012; Xu et al., 2018); this symmetry likely arose from the duplication of a monomeric ancestral channel (Durell and Guy, 1999). The selectivity filter lining the pore of Ktr and TrK and class 2 HKT proteins is composed of four glycine residues. In class 1 HKTs the first glycine within the predicted selectivity filter is substituted with serine (Mäser et al., 2002); the general lack of K^{+} permeability in this clade has been linked to the presence of this glycine substitution (Gly for Ser) (Uozumi et al., 2000; Mäser et al., 2002; Platten et al., 2006; Cotsaftis et al., 2012; Waters et al., 2013); but the exact molecular mechanism underlying this block is to be determined. While the Ser-Gly-Gly-Gly motif dictates the selectivity in class 1 HKTs, other residues are known to disrupt transport. Our recent work with both HvHKT1;5 and TaHKT1;5-D has shown that a leucine to proline substitution at position 189 or 190, respectively, disturbed the characteristic plasma membrane localization, Na^{+} transport and the ability to confer shoot Na^{+} exclusion (Borjigin et al., 2020; Houston et al., 2020).

Here, we further characterise HKT1;5 proteins underlying two major salt tolerance associated loci, *TmHKT1;5-A* (*Nax2*) and *TaHKT1;5-D* (*Kna1)* from *T. monococcum and T. aestivum*, respectively. We were surprised to find that both TmHKT1;5-A and TaHKT1;5-D in fact encode dual affinity Na^{+}-transporters and that their dual affinity Na^{+} transport can be blocked by raising the external K^{+} concentration. We further propose that the adjoining residues within the selectivity filter cause this block by the virtue of a higher number of van der Waals interactions with the K^{+} ion, than with Na^{+}. Thus, the Na^{+} ion is capable of traversing the selectivity filter, while K^{+} causes a block. This is the first report that Na^{+} transport has two affinities in the HKT1 clade and demonstrates that dual affinity transport is a common property of both clades of the HKT family.

2 | MATERIALS AND METHODS

Brief methods for cloning of *TmHKT1;5-A* (DQ646332) and *TaHKT1;5-D* (DQ646338) as well as its functional characterization in heterologous expression systems were described Munns et al. (2012) and Byrt et al. (2014). Further details are included here.

2.1 | Two-electrode voltage clamp recording in *X. laevis* oocytes

Oocyte recording followed the methods as described in Munns et al. (2012) and Byrt et al. (2014). Briefly, 46 nl/23 ng of cRNA or equal volumes of RNA-free water were injected into oocytes, followed by an incubation for 48 hr before recording. Membrane currents were recorded in the HMg solution (6 mM $MgCl_2$, 1.8 mM $CaCl_2$, 10 mM MES and pH 6.5 adjusted with a TRIS base) ± Na^{+} glutamate and/or K^{+} glutamate as indicated in relevant Figures. All solution osmolarities were adjusted using mannitol at 220–240 mOsmol kg^{-1}.

2.2 | Construction of 3D models of TaHKT1;5D in complex with Na^{+} and K^{+} ions

The most suitable template for TaHKT1;5D, the KtrB K^{+} transporter from *B. subtilis* (Protein Data Bank accession 4J7C, chain I) (Vieira-Pires et al., 2013), was identified as previously described (Xu et al., 2018). The KtrB K protein was crystallized in the presence of KCl, hence the structure contains a K^{+} ion in the selectivity filter region. This ion was substituted by Na^{+} during modeling of TaHKT1;5D that transport Na^{+} at a greater rate than K^{+} (Xu et al., 2018). 3D structural models in complex with Na^{+}, and K^{+} were generated using Modeller 9v16 (Šali and Blundell, 1993) on a Linux station running the Fedora 12 operating system, as previously described (Cotsaftis et al., 2012; Waters et al., 2013; Xu et al., 2018). During 3D modeling, attention was paid to ionic radii of Na^{+}, and K^{+}, whose topology and parameter

data were taken from CHARMM (Brooks et al., 2009), as defined in toppar_water_ions.str (Beglov and Roux, 1994). In each case, a total of 100 models were generated that were scored by Modeller 9v19 using the modeller objective function (Shen and Sali, 2006), the discrete optimized protein energy function (Eswar et al., 2008), PROCHECK (Laskowski et al., 1993), ProSa 2003 (Sippl, 1993) and FoldX (Schymkowitz et al., 2005). Best scoring models constructed in Modeller 9v19 were further subjected to energy minimization using the knowledge-based Yasara2 forcefield (bond distances, planarity of peptide bonds, bond angles, Coulomb terms, dihedral angles, and van der Waals forces) (Krieger et al., 2004), combined with the particle-mesh-Ewald (PME) energy function for long range electrostatics (cut-off 8.0 Å) to obtain smoothed electrostatic potentials. To correct covalent geometry, the conformational stress was removed by a short steepest descent minimization (time 5000 fs, 1 ft time steps, 298 K), followed by simulated annealing (time step 1 fs, atom velocities scaled down by 0.9 every 10th step) until convergence was achieved (710 steps) with energy improvement of less than 0.05 kJ/mol per atom during 200 steps (Krieger et al., 2009). Structural images were generated with PyMOL Molecular Graphics System V1.8.2.0 (Schrődinger LLC). Permeation channels and path bottlenecks in both TaHKT1;5D ionic complexes were calculated using the Mole algorithm, embedded in PyMol (Petřek et al., 2007), but using the x-y-z coordinates of Na^+ or K^+ as specifications for starting points.

3 | RESULTS

3.1 | K^+ sensitivity of TmHTK1;5-A and TaHKT1;5-D

Previously, it was shown that inward Na^+ transport of both TmHKT1;5-A and TaHKT1;5-D was inhibited by $[K^+]_{ext}$ (Munns et al., 2012; Byrt et al., 2014). Here, we further compared the K^+-sensitivity of TmHKT1;5-A and TaHKT1;5-D (Figure 1). An increase in $[K^+]_{ext}$ to 30 mM reduced the channel inward conductance (i.e., <100 mV) of

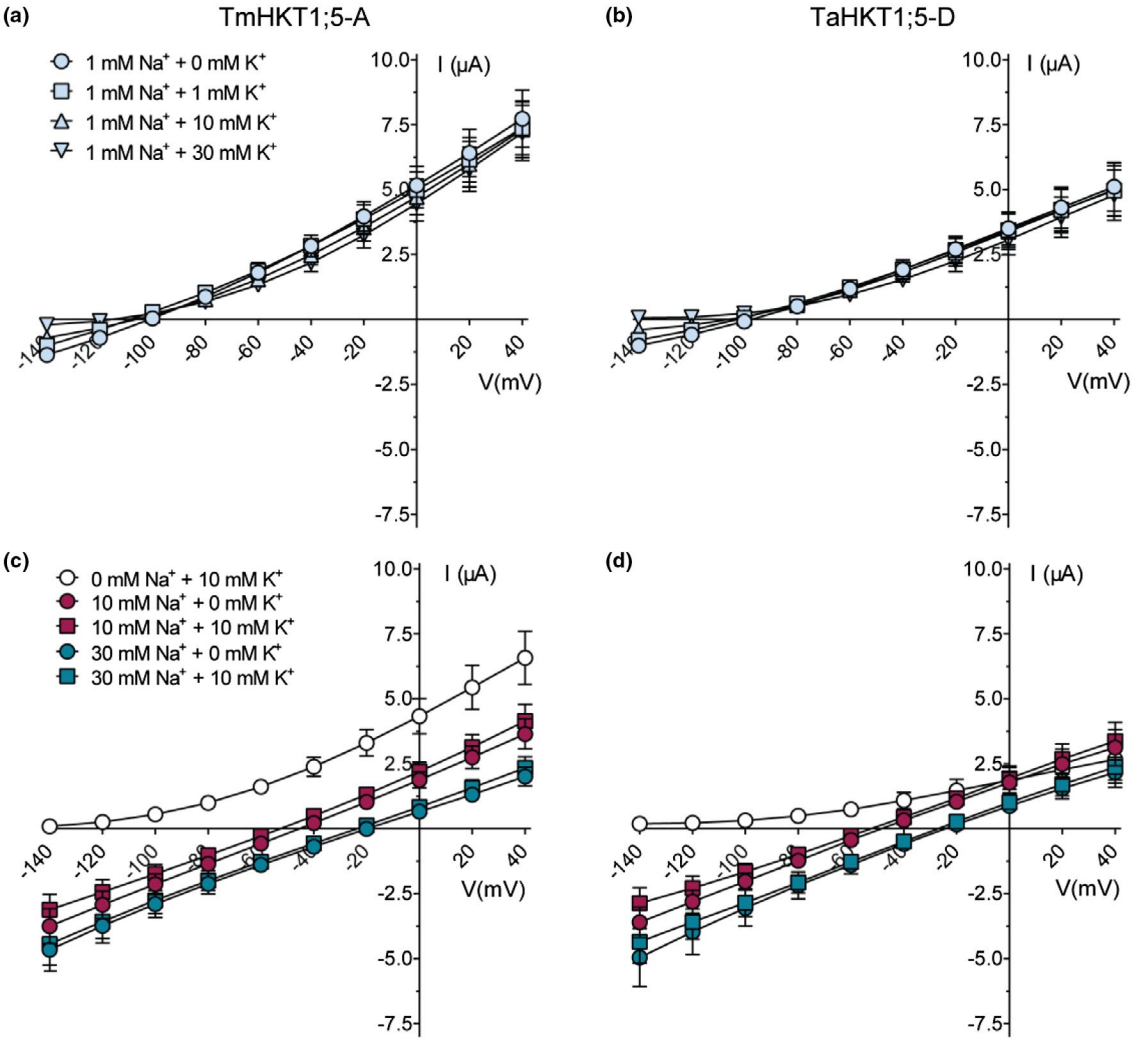

FIGURE 1 K^+-sensitivity of Na^+ currents carried by TmHKT1;5-A and TaHKT1;5-D. (a–d), current-voltage (I/V) curves of Na^+ currents recorded from *X. laevis* oocytes expressing *TmHKT1;5-A* (a and c) and *TaHKT1;5-D* (b and d) in 1 mM Na^+ plus 0–30 mM K^+ (a and b), or 0–30 mM Na^+ solutions with or without 10 mM K^+ (c and d). Mean ± SEM, $n = 5–6$

TmHKT1;5-A by approximately 75% in a 1 mM Na^+ ($[Na^+]_{ext}$) bath solution; similarly this amount of K^+ inhibited that of TaHKT1;5-D up to 95 % (Figures 1a,b and 2). However, such Na^+-inhibition by K^+ was gradually decreased by increasing $[Na^+]_{ext}$ (Figures 1 and 2). For instance, 10 mM $[K^+]_{ext}$ suppressed the channel inward conductance of TmHKT1;5-A by 43.5% in 1 mM $[Na^+]_{ext}$ and by 16.5% in 10 mM $[Na^+]_{ext}$; it similarly reduced the TaHKT1;5-D inward conductance by 57% in 1 mM $[Na^+]_{ext}$ and by 23% in 10 mM $[Na^+]_{ext}$ (Figures 1 and 2). When $[Na^+]_{ext}$ was increased to 30 mM, the channel inward conductance of TmHKT1;5-A was insensitive to $[K^+]_{ext}$, whereas that of TaHKT1;5-D was inhibited (Figure 2).

The increase in $[K^+]_{ext}$ from 0 to 10 mM did not significantly change the reversal potential of TmHKT1;5-A or TaHKT1;5-D; all reversal potentials were close to the theoretical equilibrium potential for Na^+ under all conditions (Figure 3a,b). Moreover, the observed shift in reversal potential was close to the theoretical Nernst shift for Na^+, regardless of the presence or absence of 10 mM $[K^+]_{ext}$ (Figure 3). This suggests that neither of transporter proteins were permeable to K^+.

3.2 | Dual affinity transport of Na^+ by TmHTK1;5-A and TaHKT1;5-D

The affinity for Na^+ transport of TmHKT1;5-A was previously reported to be ~four-fold higher than the Na^+-transport affinity of TaHKT1;5-D (Munns et al., 2012; Byrt et al., 2014; Xu et al., 2018), which we confirm here (Figure 4a,b). On closer examination, we found a property that has not been described before. When lower

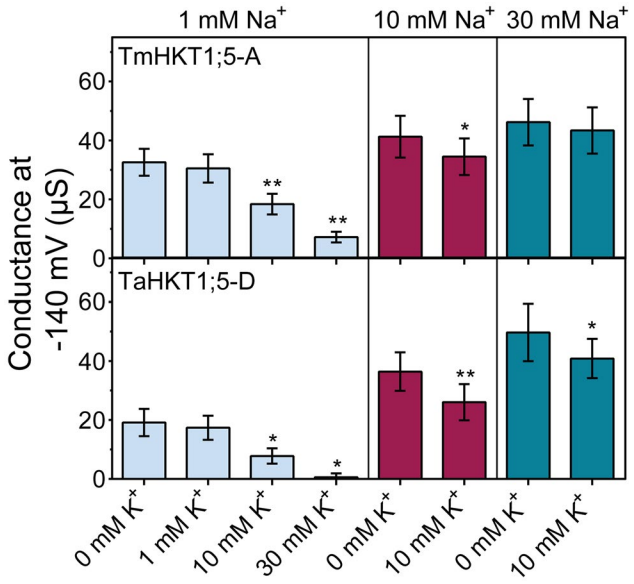

FIGURE 2 Channel conductance of TmHKT1;5-A and TaHKT1;5-D. The channel conductance of TmHKT1;5-A and TaHKT1;5-D was calculated from Figure 1, based on the slope of curve between −140 mV and −120 mV, statistical difference was determined by Students' *t* test, $^*p < .05$ and $^{**}p < .01$

concentrations of $[Na^+]_{ext}$ were present it was clear that the concentration dependence of inward Na^+ currents could be fitted by two components, for both TmHKT1;5-A and TaHKT1;5-D (Figure 4). For TmHKT1;5-A, the high affinity component of Na^+ transport had a K_m of 18.4 μM ± 0.1 μM when $[Na^+]_{ext}$ was below 0.1 mM ($K_{m\ (<0.1\ Na)}$), whereas at concentrations of Na^+ above 0.1 mM the K_m was 1.0 ± 0.2 mM ($K_{m\ (>0.1\ Na)}$) (Figure 4a). The K_m for the higher affinity component of inward Na^+ transport for TaHKT1;5-D was 15.3 μM ± 0.9 μM when $[Na^+]_{ext}$ was lower than 0.1 mM ($K_{m\ (<0.1\ Na)}$), whilst the lower affinity phase had a K_m of 4.3 ± 0.5 mM when $[Na^+]_{ext}$ was higher than 0.1 mM ($K_{m\ (>0.1\ Na)}$) (Figure 4b).

We examined the extent of K^+-inhibition of both the lower and higher affinity components of the inward Na^+ currents when $[K^+]_{ext}$ was 10 mM. The (normalized) inward Na^+ current carried by both proteins was significantly suppressed by 10 mM $[K^+]_{ext}$, resulting in negligible inward Na^+ transport by TmHKT1;5-A and TaHKT1;5-D in presence of $[Na^+]_{ext}$ below 0.1 mM (Figure 4c,d). In the presence of 10 mM $[K^+]_{ext}$ it was now possible to fit the concentration dependence of inward current through TmHKT1;5-A and TaHKT1;5-D with one component. The K_m values of both TmHKT1;5-A and TaHKT1;5-D were decreased approximately by 2.5-fold by 10 mM $[K^+]_{ext}$ (Figure 4e,f).

3.3 | Structural modeling of TaHKT1;5-D

Three-dimensional structural models of TaHKT1;5-D were generated to explore why K^+ does not traverse the pore but instead blocks the Na^+ currents, using the KtrB K^+ transporter from *B. subtilis* as a template (Vieira-Pires et al., 2013; Xu et al., 2018). The KtrB K^+ protein was crystallized in the presence of KCl, hence the original structure contained a K^+ ion in the selectivity filter region. This ion was substituted by Na^+ during modeling of TaHKT1;5-D as it transports Na^+ but not K^+ (Xu et al., 2018). Ramachandran analysis indicated that the template and TaHKT1;5-D models generated in complex with Na^+, and K^+ had satisfactory stereo-chemical quality; Ramachandran plots showed only two residues positioned in disallowed regions (0.5% of all residues, except of Gly and Pro residues). Average G-factors (measures of correctness of dihedral angles and main-chain covalent forces of protein molecules) calculated by PROCHECK of the template and TaHKT1;5-D models with K^+ and Na^+ were 0.06. −0.18, and −0.13, respectively. The ProSa 2003 analysis of z-scores (−8.4; −6.0, and −5.8) indicated that template and modeled structures with K^+ and Na^+ had acceptable conformational energies.

The TaHKT1;5-D model in complex with Na^+ showed that the Na^+ ion coordination sphere had trigonal bipyramidal geometry, as defined in the NEIGHBORHOOD SQL database (Zheng et al., 2014), with the coordination number 5. Na^+ interacted with Val76, Asn231, Cys232, His351, and Asn455 (all carbonyl oxygens), that lie near the selectivity filter residues Ser78, Gly233, Gly353 and Gly457 (Figure 5a). Conversely, the TaHKT1;5-D model in complex with K^+ showed that the K^+ ion coordination sphere had octahedral geometry

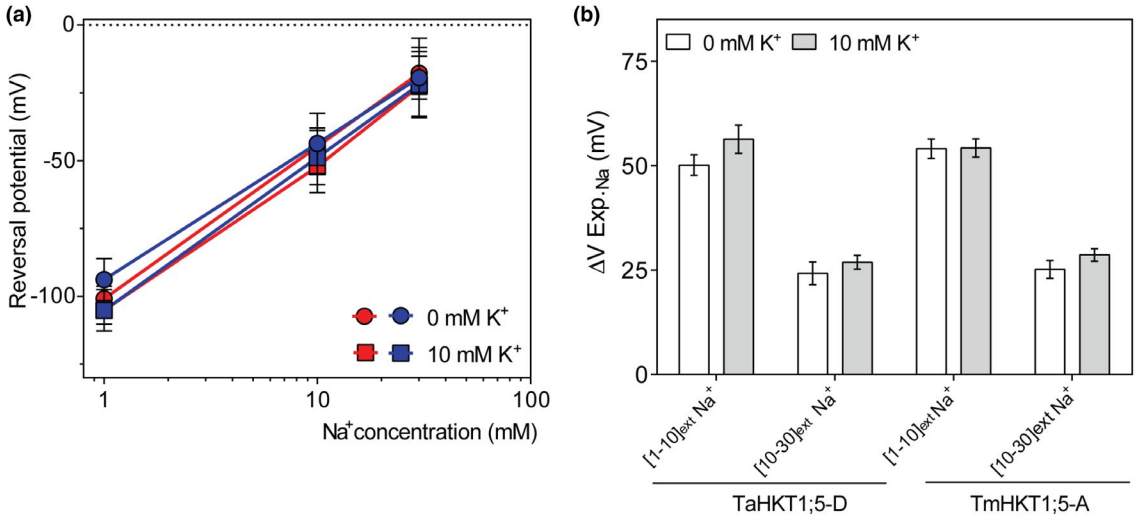

FIGURE 3 Shift in reversal potential of TmHKT1;5-A and TaHKT1;5-D in response to changes in $[Na^+]_{ext}$ and $[K^+]_{ext}$. (a), Reversal potential of currents in *X. laevis* oocytes expressing *TmHKT1;5-A* and *TaHKT1;5-D* derived from Figure 1. (b), Reversal potential of Na^+ currents plotted against theoretical Nernst potential derived from internal concentrations measured in Munns et al. (2012) and Byrt et al., (2014) at the used. Nernst shift in oocytes expressing *TmHKT1;5-A* and *TaHKT1;5-D* from 1 mM to 10 mM Na^+ ($[1\text{-}10]_{ext}$ Na^+) and 10 mM to 30 mM Na^+ ($[10\text{-}30]_{ext}$ Na^+) with or without 10 mM $[K^+]_{ext}$, $\Delta Exp._{Na}$ = experimentally measured shift in reversal potential for Na+, the theortectical equilibrium (or Nernst) potential for Na^+ was 57.7 mV and 26.9 mV, respectively for $[1\text{-}10]_{ext}$ Na^+ and $[10\text{-}30]_{ext}$ Na^+, refers to Munns et al. (2012)

(Zheng et al., 2014) with the coordination number 6; K^+ interacted with Val76, Asn231, Cys232, His351, Asn455, and Val456, that were also in the close proximity of selectivity filter residues (Figure 5b). Although none of the selectivity filter residues participated in the direct contacts with metals, Cα carbons tend to make shorter contacts with Na^+ than with K^+, that may reflect spatial adjustments of the lower ionic radius of Na^+ than that of K^+. Ionic coordination spheres and Na^+ and K^+ distances of residues were evaluated using the Metal Binding Site Validation Server (Zheng et al., 2014) that utilizes more than 500 Protein Data Bank accession numbers. Ionic coordination spheres and binding modes were found to be acceptable, and ionic distances were within the following ranges: for Na^+ ranged between 2.3 and 2.6 Å; for K^+ were between 2.6 and 2.9 Å (Figure 5, right panels).

4 | DISCUSSION

Oocytes expressing *TmHKT1;5-A* or *TaHKT1;5-D* have been previously reported to undergo no obvious change in their reversal potential regardless of the presence or absence of K^+ in bath solution. Interestingly, both transporters had differential sensitivity to external $[K^+]_{ext}$. Whilst K^+ block occurs for TmHKT1;5-A mediating inward transport it was not evident at $[Na^+]_{ext}$ above 10 mM, whereas this inhibition did happen for TaHKT1;5-D up to 30 mM $[Na^+]_{ext}$ (Figure 2) (Munns et al., 2012; Byrt et al., 2014). This differential inhibition effect of K^+ upon Na^+ transport at high $[Na^+]_{ext}$ by TaHKT1;5-D may result from a range of factors, that govern the rates of Na^+ and K^+ binding and subsequent Na^+ transport. A variety of factors could control the transport of Na^+ and the preliminary displacement of competing K^+ with a consequent energetic cost, before Na^+ passes desolvated or less-well hydrated than competing K^+. Examples include free-energy variations between ions in binding sites relative to the corresponding quantity in bulk water, differences in selectivity filters solvent exposures (or dielectric constants), overall pore rigidity/stiffness (Dudev and Lim, 2010), structural changes within funnels and selectivity filters due to residue re-orientation, differences in the hydration (coordination) numbers of Na^+ and K^+ (Na^+ and K^+ bind six and seven water molecules, respectively) (Rowley and Roux, 2012) and the alterations on the rates of Na^+ or K^+ de-solvation (Degrève et al., 1996). It is, therefore, plausible to expect that both ions would compete for binding sites within HKT funnel regions, yielding ion-protein binding sites with differential binding strengths.

Here, we conduct advanced 3D homology modeling and include explicit ionic radii of Na^+ and K^+ based on the CHARMM force field (Brooks et al., 2009), rather than a traditional rigid body-type modeling for ligands. The aim has been to refine the previous structural model of HKT1;5 to show that the current model contains a pore that allows the passage of Na^+ but not K^+ (Cotsaftis et al., 2012; Waters et al., 2013; Xu et al., 2018). This is consistent with the functional observations in this and previous studies (Munns et al., 2012; Byrt et al., 2014). Previously it was suggested that the Gly-Gly-Gly-Gly motif is important in coordinating the K^+ in Ktr/TrK transporters and in conferring dual Na^+-K^+ transport in HKT2 transporters (Durell and Guy, 1999; Mäser et al., 2002). Here, our structural modeling suggests that the serine residue within the Ser-Gly-Gly-Gly selectivity motif directly interacts and binds Na^+ (Figure 5b). Furthermore, our model suggests, despite ionic distances being shorter for Na^+ than for K^+, that K^+ could be bound more strongly due to a higher coordination pattern (Figure 5a,b-right panels). Obviously, during

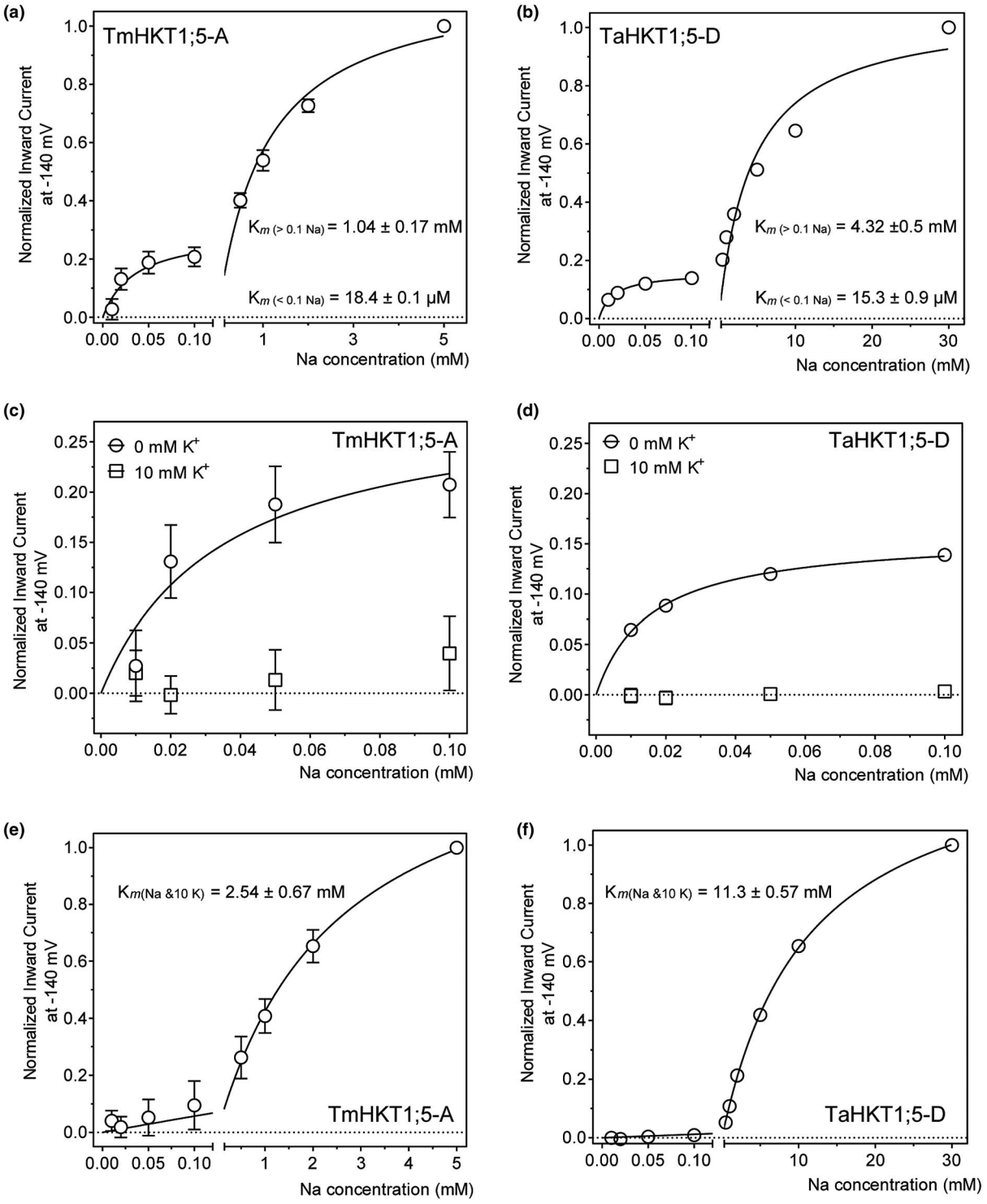

FIGURE 4 Transport affinity of TmHKT1;5-A and TaHKT1;5-D in *X. laevis* oocytes. (a and b), dual Na^+-transport affinity of TmHKT1;5-A and TaHKT1;5-D in *X. laevis* oocytes, plotted as normalized currents at −140 mV as shown against a series of Na^+ glutamate solutions. (c and d), high affinity phase of TmHKT1;5-A and TaHKT1;5-D in absence and presence of 10 mM $[K^+]_{ext}$. Data represented in A, B, and C as mean ± SEM, $n = 4$ for (a); $n = 7$ for (b); $n = 4$ of 0 mM K^+ and $n = 5$ of 10 mM K^+ for (c); and $n = 7$ of 0 mM K^+ and $n = 4$ of 10 mM K^+ for (d). (e and f), Na^+-transport affinity of TmHKT1;5-A and TaHKT1;5-D in *X. laevis* oocytes, plotted as normalized currents at −140 mV as shown against a series of Na^+ glutamate solutions with an additional 10 mM K^+ glutamate, $n = 5$ for (e) and $n = 4$ for (f). The (normalized) inward Na^+ current carried by both proteins was significantly suppressed by 10 mM $[K^+]_{ext}$, resulting in negligible inward Na^+ transport by TmHKT1;5-A and TaHKT1;5-D in presence of $[Na^+]_{ext}$ below 0.1 mM (c and d)

binding, K^+ takes an advantage of its larger ionic radius: 152 picometer (pm), compared to that of Na^+ (116 pm); these parameters reflects empirical atomic radii of K (220 pm) and Na (180 pm). We assume that under the high concentrations of K^+, this ion may outcompete Na^+

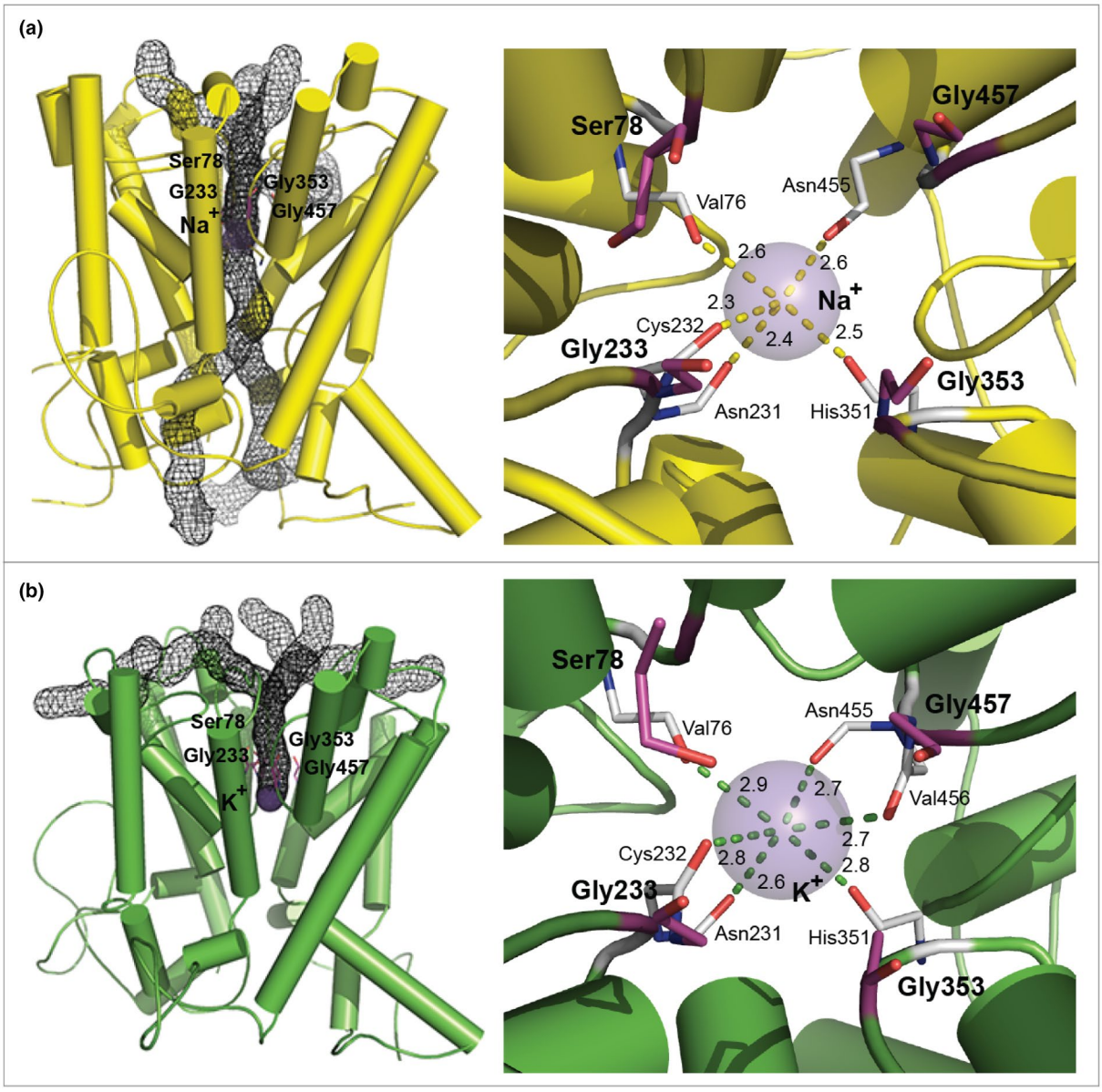

FIGURE 5 Molecular models of TaHKT1;5D in complex with Na^+ (a) and K^+ (b) ions. (a-b; left panels) Cartoon representations of TaHKT1;5-D illustrate overall protein folds with cylindrical α-helices, and translocating permeation channels (black mesh) calculated at path bottlenecks using Mole (Petřek et al., 2007). Na^+ (a) and K^+ (b) ions are shown as purple spheres located within the selectivity filter residues Ser78, Gly233, Gly353 and Gly457 (colored in cpk magenta), and other neighboring residues. Na^+ is likely to enter and exit the permeation trajectory from several points on both sides of the transporter, but always by-passes the selectivity filter constriction. K^+ enters the selectivity filter and effectively blocks the permeation at the constriction bottleneck. For clarity, membrane α-helices are only shown. (a-b; right panels) Detailed views of coordination spheres of Na^+ and K^+ ions, and ionic interactions with residues adjoining the selectivity filter residues Ser78, Gly233, Gly353, and Gly457. The ionic distances of 2.3–2.8 Å for Na^+ between Val76, Ser77, Ser78, Asn231, Cys232, and His351, and of 2.6–2.9 Å for K^+ between Val76, Asn231, Cys232, His351, Asn455, and Val456, are formed between carbonyl oxygens of residues (in sticks in atomic colors). The K^+ ion effectively blocks the permeation channel through the protein pore at the constriction bottleneck point, contrary to Na^+

and would become bound in the selectivity filter, thus effectively blocking Na^+ transport. This is illustrated by calculating permeation channels in both complexes, using the Mole Voronoi algorithm, that predicts permeation trajectories and identifies path bottlenecks. From the calculated permeation paths, it could be deduced that K^+ effectively blocks the permeation channel through the major gating protein pore, contrary to Na^+. It is also obvious that Na^+ is likely to enter and exit the permeation trajectory from several points on both sides of the transporter, but always by-passes the selectivity filter constriction. Both ions arrive at the funnel of HKT proteins in solvated (hydrated) forms. While the hydration number for Na^+ is 6, that for K^+ is 7 at ambient temperature (Rowley and Roux, 2012; Ma, 2014). The significance of the seven-fold water coordination for K^+ is that this solvated complex may form a stronger hydrogen-bond

interaction pattern (in funnels of HKT proteins), and would be de-solvated with a higher energy input and thus slower that the Na^+ solvated complex (Degrève et al., 1996). It is also plausible to expect that both solvated ion complexes would compete for binding sites within HKT funnel regions with different binding strengths. All in all, this would contribute to the blockage of the pore entry of HKT transporters by K^+.

Potassium permeability for HKT1 transporters has only been reported once for the proteins that have been characterised in *X. laevis* oocytes. The transporters EcHKT1;1 and EcHKT1;2 allow permeation of both K^+ and Na^+ (Liu et al., 2001). Interestingly, when 3D models of the Na^+ selective OsHKT1;5 and K^+ permeable EcHKT1;2 were constructed and compared the pore size was predicted to be 0.2 Å larger in EcHKT1;2 (and that of OsHKT1;5 and TaHKT1;5-D), which would more than account for the weaker interactions with K^+ and allow this larger ion to pass through the pore as well as Na^+ (Waters et al., 2013). Without advanced 3D modeling of each and every transporter in the HKT family, to demonstrate how the selectivity filter forms in the context of the remainder of the protein, it would not be possible to predict which other HKT1s may allow passage of K^+. Predictions based on sequence alone are insufficient to suggest how the two sets of proteins evolved their individual Na^+ and K^+ transport characteristics (David et al., 2019). An extension of the model to include other HKT proteins, a greater survey of structure-function relationships and mutations of key residues to predict functionally relevant residues and evolutionary relationships will be the focus of further studies.

Two affinity ranges for Na^+ transport have been detected in the HKT family previously, but only for HKT2 transporters e.g. OsHKT2;1, OsHKT2;2, OsHKT2;4, and HvHKT2;1 (Schachtman and Schroeder, 1994; Rubio et al., 1995; Jabnoune et al., 2009; Yao et al., 2010; Horie et al., 2011; Sassi et al., 2012). For instance, for OsHKT2;2, when K^+ is present, the transport of Na^+ is K^+-dependent and displays a high affinity (K_m = 0.077 mM), whereas showing a lower affinity when absence of K^+ (K_m = 16 mM) (Rubio et al., 1995; Yao et al., 2010). OsHKT2;1 also acquires two phases of Na^+-transport affinity, whose K_m for Na^+ is, respectively, 9.5 μM at $[Na^+]_{ext}$ below 1 mM and is 2.2 mM at $[Na^+]_{ext}$ > 1 mM (Jabnoune et al., 2009). The K^+ transport catalyzed by HvHKT2;1 is affected by both $[Na^+]_{ext}$ and $[K^+]_{ext}$, such as a decrease in its K^+ transport affinity from 30 μM down to 3.5 mM by $[Na^+]_{ext}$ increased from 0.5 to 30 mM and a greatly reduced channel conductivity for K^+ by increasing $[K^+]_{ext}$ above ~3 mM (Mian et al., 2011). This is the first time that dual affinity characteristics have been reported for the HKT1 family (Figure 4). Considering the relatively high homology between both clades (58% similarity/41% identity between TaHKT1;5 and TaHKT2;1) it is perhaps not surprising that both clades can confer dual affinity transport. How and why such ability has evolved and is conferred structurally is still to be determined.

In summary, we have detected that TaHKT1;5-D and TmHKT1;5-A can both conduct high and low affinity Na^+ transport, both phases can be blocked by external K^+ with the low affinity component of Na^+ transport for TmHKT1;5-A being less inhibited by external K^+ than TaHKT1;5-D (Figure 4). The two K_m at the high affinity phases were similar, but the K_m value for the low affinity component of TmHKT1;5-A was always ~4 fold lower regardless of the absence or presence of $[K^+]_{ext}$ (Figure 4) (Munns et al., 2012; Byrt et al., 2014). TmHKT1;5-A has been shown to be more effective in conferring shoot Na^+ exclusion to wheat compared to TaHKT1;5-D (James et al., 2012). We propose that the higher affinity (with half-maximal activity nearer 1 mM compared to 4 mM), and a lower sensitivity to $[K^+]_{ext}$ are both characteristics that can help confer better shoot Na^+ exclusion, which is a property that can lead to greater salt tolerance in the field for wheat (James et al., 2011; James et al., 2012; Munns et al., 2012).

CONFLICT OF INTEREST

The authors declare no conflict of interest associated with the work described in this.

AUTHOR CONTRIBUTION

All authors conceived the project. BX performed all electrophysiology, MH performed 3D structural modeling. All authors wrote the manuscript.

ORCID

Bo Xu https://orcid.org/0000-0002-7583-2384
Maria Hrmova https://orcid.org/0000-0002-3545-0605
Matthew Gilliham https://orcid.org/0000-0003-0666-3078

REFERENCES

Almeida, P., de Boer, G.-J., & de Boer, A. H. (2014). Differences in shoot Na^+ accumulation between two tomato species are due to differences in ion affinity of HKT1;2. *Journal of Plant Physiology*, *171*, 438–447.

Almeida, P., Feron, R., de Boer, G.-J., & de Boer, A. H. (2014). Role of Na^+, K^+, Cl^-, proline and sucrose concentrations in determining salinity tolerance and their correlation with the expression of multiple genes in tomato. *AoB Plants*, *6*, plu039.

Asins, M. J., Villalta, I., Aly, M. M., Olias, R., Álvarez De Morales, P., Huertas, R., Li, J., Jaime-Pérez, N., Haro, R., & Raga, V. (2013). Two closely linked tomato HKT coding genes are positional candidates for the major tomato QTL involved in Na^+/K^+ homeostasis. *Plant, Cell & Environment*, *36*, 1171–1191.

Beglov, D., & Roux, B. (1994). Finite representation of an infinite bulk system: Solvent boundary potential for computer simulations. *The Journal of Chemical Physics*, *100*, 9050–9063.

Ben Amar, S., Brini, F., Sentenac, H., Masmoudi, K., & Véry, A.-A. (2013). Functional characterization in *Xenopus oocytes* of Na^+ transport systems from durum wheat reveals diversity among two HKT1; 4 transporters. *Journal of Experimental Botany*, *65*, 213–222.

Borjigin, C., Schilling, R. K., Bose, J., Hrmova, M., Qiu, J., Wege, S., Situmorang, A., Brien, C., Berger, B., & Gilliham, M. (2020). A single nucleotide substitution in TaHKT1; 5-D controls shoot Na^+ accumulation in bread wheat. *Plant, Cell & Environment*, *43*, 2158–2171.

Brooks, B. R., Brooks, C. L., MacKerell, A. D., Nilsson, L., Petrella, R. J., Roux, B., Won, Y., Archontis, G., Bartels, C., Boresch, S., & Caflisch, A. (2009). CHARMM: The biomolecular simulation program. *Journal of Computational Chemistry*, *30*, 1545–1614.

Byrt, C. S., Xu, B., Krishnan, M., Lightfoot, D. J., Athman, A., Jacobs, A. K., Watson-Haigh, N. S., Plett, D., Munns, R., & Tester, M. (2014). The

Na^+ transporter, TaHKT1;5-D, limits shoot Na^+ accumulation in bread wheat. *The Plant Journal*, *80*, 516–526.

Campbell, M. T., Bandillo, N., Al Shiblawi, F. R. A., Sharma, S., Liu, K., Du, Q., Schmitz, A. J., Zhang, C., Véry, A.-A., & Lorenz, A. J. (2017). Allelic variants of OsHKT1; 1 underlie the divergence between indica and japonica subspecies of rice (*Oryza sativa*) for root sodium content. *PLoS Genetics*, *13*, e1006823.

Cao, Y., Liang, X., Yin, P., Zhang, M., & Jiang, C. (2019). A domestication-associated reduction in K^+-preferring HKT transporter activity underlies maize shoot K^+ accumulation and salt tolerance. *New Phytologist*, *222*, 301–317.

Corratgé-Faillie, C., Jabnoune, M., Zimmermann, S., Véry, A.-A., Fizames, C., & Sentenac, H. (2010). Potassium and sodium transport in non-animal cells: The Trk/Ktr/HKT transporter family. *Cellular and Molecular Life Sciences*, *67*, 2511–2532.

Cotsaftis, O., Plett, D., Shirley, N., Tester, M., & Hrmova, M. (2012). A two-staged model of Na^+ exclusion in rice explained by 3D modeling of HKT transporters and alternative splicing. *PLoS One*, *7*, e39865.

David, R., Byrt, C. S., Tyerman, S. D., Gilliham, M., & Wege, S. (2019). Roles of membrane transporters: Connecting the dots from sequence to phenotype. *Annals of Botany*, *124*, 201–208.

Degrève, L., Vechi, S. M., & Junior, C. Q. (1996). The hydration structure of the Na^+ and K^+ ions and the selectivity of their ionic channels. *Biochimica et Biophysica Acta - Bioenergetics*, *1274*, 149–156.

Dudev, T., & Lim, C. (2010). Factors governing the Na^+ vs K^+ selectivity in sodium ion channels. *Journal of the American Chemical Society*, *132*, 2321–2332.

Durell, S. R., & Guy, H. R. (1999). Structural models of the KtrB, TrkH, and Trk 1, 2 symporters based on the structure of the KcsA K^+ channel. *Biophysical Journal*, *77*, 789–807.

Eswar, N., Eramian, D., Webb, B., Shen, M.-Y., & Sali, A. (2008). Protein structure modeling with MODELLER. In B. Kobe, M. Guss, & T. Huber (Eds.), *Structural proteomics*. Methods in molecular biology (Vol. *426*, pp. 145–159). Springer.

Henderson, S. W., Dunlevy, J. D., Wu, Y., Blackmore, D. H., Walker, R. R., Edwards, E. J., Gilliham, M., & Walker, A. R. (2018). Functional differences in transport properties of natural HKT 1; 1 variants influence shoot Na^+ exclusion in grapevine rootstocks. *New Phytologist*, *217*, 1113–1127.

Horie, T., Brodsky, D. E., Costa, A., Kaneko, T., Schiavo, F. L., Katsuhara, M., & Schroeder, J. I. (2011). K^+ transport by the OsHKT2; 4 transporter from rice with atypical Na^+ transport properties and competition in permeation of K^+ over Mg^{2+} and Ca^{2+} ions. *Plant Physiology*, *156*, 1493–1507.

Houston, K., Qiu, J., Wege, S., Hrmova, M., Oakey, H., Qu, Y., Smith, P., Situmorang, A., Macaulay, M., Flis, P., & Bayer, M. (2020). Barley sodium content is regulated by natural variants of the Na^+ transporter HvHKT1; 5. *Communications Biology*, *3*, 1–9.

Ismail, A. M., & Horie, T. (2017). Genomics, physiology, and molecular breeding approaches for improving salt tolerance. *Annual Review of Plant Biology*, *68*, 405–434.

Jabnoune, M., Espeout, S., Mieulet, D., Fizames, C., Verdeil, J.-L., Conéjéro, G., Rodríguez-Navarro, A., Sentenac, H., Guiderdoni, E., & Abdelly, C. (2009). Diversity in expression patterns and functional properties in the rice HKT transporter family. *Plant Physiology*, *150*, 1955–1971.

James, R. A., Blake, C., Byrt, C. S., & Munns, R. (2011). Major genes for Na^+ exclusion, *Nax1* and *Nax2* (wheat *HKT1; 4* and *HKT1; 5*), decrease Na^+ accumulation in bread wheat leaves under saline and waterlogged conditions. *Journal of Experimental Botany*, *62*, 2939–2947.

James, R. A., Blake, C., Zwart, A. B., Hare, R. A., Rathjen, A. J., & Munns, R. (2012). Impact of ancestral wheat sodium exclusion genes *Nax1* and *Nax2* on grain yield of durum wheat on saline soils. *Functional Plant Biology*, *39*, 609–618.

James, R. A., Davenport, R. J., & Munns, R. (2006). Physiological characterization of two genes for Na^+ exclusion in durum wheat, *Nax1* and *Nax2*. *Plant Physiology*, *142*, 1537–1547.

Krieger, E., Darden, T., Nabuurs, S. B., Finkelstein, A., & Vriend, G. (2004). Making optimal use of empirical energy functions: Force-field parameterization in crystal space. *Proteins*, *57*, 678–683.

Krieger, E., Joo, K., Lee, J., Lee, J., Raman, S., Thompson, J., Tyka, M., Baker, D., & Karplus, K. (2009). Improving physical realism, stereochemistry, and side-chain accuracy in homology modeling: Four approaches that performed well in CASP8. *Proteins*, *77*, 114–122.

Lan, W.-Z., Wang, W., Wang, S.-M., Li, L.-G., Buchanan, B. B., Lin, H.-X., Gao, J.-P., & Luan, S. (2010). A rice high-affinity potassium transporter (HKT) conceals a calcium-permeable cation channel. *Proceedings of the National Academy of Sciences of the United States of America*, *107*, 7089–7094.

Laskowski, R. A., MacArthur, M. W., Moss, D. S., & Thornton, J. M. (1993). PROCHECK: A program to check the stereochemical quality of protein structures. *Journal of Applied Crystallography*, *26*, 283–291.

Liu, W., Fairbairn, D. J., Reid, R. J., & Schachtman, D. P. (2001). Characterization of two HKT1 homologues from *Eucalyptus camaldulensis* that display intrinsic osmosensing capability. *Plant Physiology*, *127*, 283–294.

Ma, H. (2014). Hydration structure of Na^+, K^+, F^-, and Cl^- in ambient and supercritical water: A quantum mechanics/molecular mechanics study. *International Journal of Quantum Chemistry*, *114*, 1006–1011.

Mäser, P., Hosoo, Y., Goshima, S., Horie, T., Eckelman, B., Yamada, K., Yoshida, K., Bakker, E. P., Shinmyo, A., & Oiki, S. (2002). Glycine residues in potassium channel-like selectivity filters determine potassium selectivity in four-loop-per-subunit HKT transporters from plants. *Proceedings of the National Academy of Sciences of the United States of America*, *99*, 6428–6433.

Mian, A., Oomen, R. J., Isayenkov, S., Sentenac, H., Maathuis, F. J., & Véry, A. A. (2011). Over-expression of an Na^+-and K^+-permeable HKT transporter in barley improves salt tolerance. *The Plant Journal*, *68*, 468–479.

Munns, R., Day, D. A., Fricke, W., Watt, M., Arsova, B., Barkla, B. J., Bose, J., Byrt, C. S., Chen, Z. H., Foster, K. J., & Gilliham, M. (2020). Energy costs of salt tolerance in crop plants. *New Phytologist*, *225*, 1072–1090.

Munns, R., & Gilliham, M. (2015). Salinity tolerance of crops–What is the cost? *New Phytologist*, *208*, 668–673.

Munns, R., James, R. A., Xu, B., Athman, A., Conn, S. J., Jordans, C., Byrt, C. S., Hare, R. A., Tyerman, S. D., Tester, M., & Plett, D. (2012). Wheat grain yield on saline soils is improved by an ancestral Na^+ transporter gene. *Nature Biotechnology*, *30*, 360–364.

Petřek, M., Košinová, P., Koča, J., & Otyepka, M. (2007). MOLE: A Voronoi diagram-based explorer of molecular channels, pores, and tunnels. *Structure*, *15*, 1357–1363.

Platten, J. D., Cotsaftis, O., Berthomieu, P., Bohnert, H., Davenport, R. J., Fairbairn, D. J., Horie, T., Leigh, R. A., Lin, H.-X., & Luan, S. (2006). Nomenclature for HKT transporters, key determinants of plant salinity tolerance. *Trends in Plant Science*, *11*, 372–374.

Ren, Z.-H., Gao, J.-P., Li, L.-G., Cai, X.-L., Huang, W., Chao, D.-Y., Zhu, M.-Z., Wang, Z.-Y., Luan, S., & Lin, H.-X. (2005). A rice quantitative trait locus for salt tolerance encodes a sodium transporter. *Nature Genetics*, *37*, 1141–1146.

Rowley, C. N., & Roux, B. T. (2012). The solvation structure of Na^+ and K^+ in liquid water determined from high level ab initio molecular dynamics simulations. *Journal of Chemical Theory and Computation*, *8*, 3526–3535.

Rubio, F., Gassmann, W., & Schroeder, J. I. (1995). Sodium-driven potassium uptake by the plant potassium transporter HKT1 and mutations conferring salt tolerance. *Science*, *270*, 1660.

Šali, A., & Blundell, T. L. (1993). Comparative protein modelling by satisfaction of spatial restraints. *Journal of Molecular Biology*, *234*, 779–815.

Sassi, A., Mieulet, D., Khan, I., Moreau, B., Gaillard, I., Sentenac, H., & Véry, A.-A. (2012). The rice monovalent cation transporter OsHKT2; 4: Revisited ionic selectivity. *Plant Physiology*, *160*, 498–510.

Schachtman, D. P., & Schroeder, J. I. (1994). Structure and transport mechanism of a high-affinity potassium uptake transporter from higher plants. *Nature*, *370*, 655–658.

Schymkowitz, J., Borg, J., Stricher, F., Nys, R., Rousseau, F., & Serrano, L. (2005). The FoldX web server: An online force field. *Nucleic Acids Research*, *33*, W382–W388.

Sentenac, H., & Bonneaud, N. (1992). Cloning and expression in yeast of a plant potassium ion transport system. *Science*, *256*, 663.

Shen, M. Y., & Sali, A. (2006). Statistical potential for assessment and prediction of protein structures. *Protein Science*, *15*, 2507–2524.

Sippl, M. J. (1993). Recognition of errors in three-dimensional structures of proteins. *Proteins*, *17*, 355–362.

Uozumi, N., Kim, E. J., Rubio, F., Yamaguchi, T., Muto, S., Tsuboi, A., Bakker, E. P., Nakamura, T., & Schroeder, J. I. (2000). The Arabidopsis HKT1 gene homolog mediates inward Na^+ currents in *Xenopus laevis* oocytes and Na^+ uptake in *Saccharomyces cerevisiae*. *Plant Physiology*, *122*, 1249–1260.

van Zelm, E., Zhang, Y., & Testerink, C. (2020). Salt tolerance mechanisms of plants. *Annual Review of Plant Biology*, *71*, 403–433.

Vieira-Pires, R. S., Szollosi, A., & Morais-Cabral, J. H. (2013). The structure of the KtrAB potassium transporter. *Nature*, *496*, 323–328.

Waters, S., Gilliham, M., & Hrmova, M. (2013). Plant high-affinity potassium (HKT) transporters involved in salinity tolerance: Structural insights to probe differences in ion selectivity. *International Journal of Molecular Sciences*, *14*, 7660–7680.

Wu, Y., Henderson, S. W., Wege, S., Zheng, F., Walker, A. R., Walker, R. R., & Gilliham, M. (2020). The grapevine NaE sodium exclusion locus encodes sodium transporters with diverse transport properties and localisation. *Journal of Plant Physiology*, *246*, 153113.

Xu, B., Waters, S., Byrt, C. S., Plett, D., Tyerman, S. D., Tester, M., Munns, R., Hrmova, M., & Gilliham, M. (2018). Structural variations in wheat HKT1; 5 underpin differences in Na^+ transport capacity. *Cellular and Molecular Life Sciences*, *75*, 1–12.

Yao, X., Horie, T., Xue, S., Leung, H.-Y., Katsuhara, M., Brodsky, D. E., Wu, Y., & Schroeder, J. I. (2010). Differential sodium and potassium transport selectivities of the rice OsHKT2; 1 and OsHKT2; 2 transporters in plant cells. *Plant Physiology*, *152*, 341–355.

Zheng, H., Chordia, M. D., Cooper, D. R., Chruszcz, M., Müller, P., Sheldrick, G. M., & Minor, W. (2014). Validation of metal-binding sites in macromolecular structures with the CheckMyMetal web server. *Nature Protocols*, *9*, 156.

How to cite this article: Xu B, Hrmova M, Gilliham M. High affinity Na^+ transport by wheat HKT1;5 is blocked by K^+. *Plant Direct*. 2020;00:1–10. https://doi.org/10.1002/pld3.275